RSC Advances

PAPER

View Article Online
View Journal | View Issue

Cite this: *RSC Adv.*, 2021, **11**, 36607

Transparent, conductive and superhydrophobic cellulose films for flexible electrode application

Yu Wang and Jin-Tian Huang *

Cellulose has shown encouraging properties in many applications, such as energy storage, optical instrument and catalysis. In particular, cellulose films have shown potential applications in flexible transparent devices and are expected to replace indium-tin oxide (ITO). However, cellulose is highly hydrophilic and electrically insulating, which limits its scope of application. In this study, the conductivity (R_s = 40.3 Ω sq^{-1}), transparency (81.4%) and superhydrophobicity (static contact angle = 153.2°, sliding angle = 4.1°) of cellulose film (CTSC-P) are reported. First, before suction filtration to prepare the film, cellulose was oxidized to improve dispersibility and mechanical strength. Then, the obtained film was hydrophobically modified by grafting long-chain silanes on the surface, followed by electrospinning and electroless plating. In general, the design is an ingenious way to manufacture transparent, conductive, and super-hydrophobic films in the future, and is transformed into a flexible electronic technically feasible device.

Received 13th September 2021
Accepted 14th October 2021

DOI: 10.1039/d1ra06865b

rsc.li/rsc-advances

1. Introduction

Materials with high conductivity and light transmittance are getting more and more attention, especially in the electronics industry including computer monitors[1–4], photovoltaic materials[5–7] and mobile phone touch screens.[8–10] ITO conductive material is made by coating a layer of indium tin oxide film on different substrates through magnetron sputtering. It is currently the most widely commercialized conductive and transparent material used in display materials. Nevertheless, it has some fatal flaws, such as high price and brittleness of indium. Those defects severely restricted the application in the field of flexible electrode materials,[11–13] which is one of the important directions for the development of visualization and display materials in the future.

Cellulose is a renewable and degradable resource with huge reserves in nature. It has attractive features and numerous derivatives. As a transparent and flexible substrate, it has shown great potential in future electronic products. Low-cost chemically modified cellulose derivatives have good flexibility, making the film dense, high transparency, and can maintain various mechanical deformation and chemical degradation. It is an excellent candidate for attaching conductive materials.[14–17] Considering that the network structure formed by long fibers has higher mechanical strength and durability, TEMPO oxidized cellulose is usually used as a flexible transparent substrate. And how to endow cellulose films conductive properties has become the focus of academia. To this end, some improved techniques have been developed to fabri-cate various materials, such as conductive polymers,[18–21] regular nanonetworks,[22–24] carbon nanotubes,[25–28] graphene oxide,[29–32] and random metal networks[33–37] to endow cellulose film conductivity to replace ITO. However, all these techniques are complex and costly due to tedious processing.

Metal nanowires have excellent photoelectric properties and have been used in touch screen displays, photovoltaic devices, electrochromic devices, and transparent or stretchable functional devices, paving the way for the replacement of ITO. However, there are still many unresolved problems, such as junction resistance between the metal nanowires. To this end, some improved technologies have been developed to produce a variety of metal grid open areas, such as bubble templates and coffee ring effect templates. However, all of these still have limitations due to the complexity of the technology, the high cost, and the dependence of various templates or cumbersome processing.[38]

Electrospinning is a mature technology that can be mass-produced under low-cost conditions recognized by the public, and can form an effective network structure on the surface of the substrate, which provides a preliminary structure for electronic conduction. Then, how to wrap these networks with conductive materials is the next question. Although electroless plating is a good method, because cellulose has strong hydrophilicity, the substrate needs to be completely immersed in the electroless plating solution during the electroless plating process, which cannot guarantee that the metallic silver is only deposited on the surface of the network to avoid opening. Area to maintain the transparency of the electrode material. In this study, we design a simple and low-cost method to obtain

College of Material Science and Art Design, Inner Mongolia Agriculture University, China. E-mail: jintian_h@163.com

transparent, conductive, and superhydrophobic cellulose films, which can be manufactured in a large area. TEMPO oxidized cellulose is used as the electrode material substrate. Cellulose microspheres and long-chain silanes cooperate to build a superhydrophobic structure. The superhydrophobic passivated coating provides a necessary foundation for activation and deposition of silver particles on the surface of the polymer network containing stannous chloride deposited by electrospinning. During the activation process, the Ag^+ are reduced to Ag particles by Sn^+ exposed on the surface of the polymer network to form reaction sites, which further catalyze the deposition of Ag particles on the entire surface of the polymer network to form a connected conductive network. As aresult, the obtained film shows a transmittance higher than 81.4% at the wavelength of visible light, and can be bent and deformed into multiple cycles without losing superhydrophobicity.

2. Experimental section

2.1 Materials

Commercial paper pulp (Pinus sylvestris) from Inner Mongolia Tianyuan wood Co., Ltd. (Hohhot, China) was used as cellulose raw materials. Commercial cellulose nanocrystals spheres (CNS), stannous chloride ($SnCl_2$), sulfuric acid (H_2SO_4), polyvinyl butyral (PVB), 2,2,6,6-tetramethylpiperidinyl-1-oxyl (TEMPO), glucose, sodium bromide (NaBr), sodium hypochlorite (NaClO), hydrochloric acid (HCl), sodium hydroxide (NaOH), silver nitrate($AgNO_3$), methyl trichlorosilane (MTCS), toluene and ethanol were all purchased from Tianjin Sinopharm Chemistry Co., Ltd. (Tianjin, China). All the above chemicals were analytical grade.

2.2 Fabrication of TEMPO oxidized cellulose film (TOC-P)

TEMPO oxidized cellulose (TOC) was obtained according to methods reported elsewhere.[39] Place the microporous filter membrane on the surface of the sand core funnel and wet it with a small amount of water to make the filter membrane and the surface of the funnel fit completely. 0.1 g of dry TOC was used to prepare a suspension and then added to the funnel. After suction filtration for a period of time, a translucent gel-like membrane was obtained, and TOC-P was obtained after drying at room temperature. The resulting TOC-P was pressure-shaped in ethanol for later use.

2.3 Fabrication of TEMPO oxidized cellulose-CNS film (TOC-CNS-P)

A micro porous filter membrane was put on the surface of the sand core funnel, wet it with a small amount of water, and make the filter membrane and the funnel surface completely fit. 0.08 g dry TOC and 0.02 g dry CNS to prepare a suspension and added into the funnel. After a period of suction filtration, a translucent gel-like membrane was obtained, and TOC-CNS-P was obtained after drying at room temperature. The resulting TOC-CNS-P was pressure-set in ethanol for subsequent use.

2.4 Superhydrophobic modification of TOC-CNS-P (H-TOC-CNS-P)

The typical manufacturing process of the three-dimensional micro-nano convex structure in the liquid phase is as follows. First of all, 10 ml of anhydrous toluene was added into a 50 ml glass beaker. Then, the TOC-CNS-P is immersed in it, and methyltrichlorosilane was added to the solvent corresponding to the definite concentration. The beaker is then exposed to air, but exposed to the chamber environment during the solution and sample introduction. When the reaction is over, the processed TOC-CNS-P was immersed in the corresponding solution several times, and then a series of rinsing of the substrate with different solvents as followed order: toluene, toluene : ethanol (1 : 1), ethanol, ethanol : deionized water (1 : 1), and finally deionized water. At last, the film was dried in a drying oven at 60 °C for 30 minutes. The H-TOC-CNS-P was obtained.

2.5 Fabrication of conductive, transparent and superhydrophobic cellulose film (CTSC-P)

Dissolved PVB (10 wt%) and $SnCl_2$ (20%) in a 1 : 1 mixed solution of dimethylacetamide (DMAC) and ethanol. Put the electrospinning solution into a 5 ml syringe with a non-contaminated syringe needle (0.5 mm in diameter). The working distance between the needle and the collector was 15 cm. Apply a voltage of 10 kV, and collect the PVB nanowire network on the surface of the H-TOC-CNS-P.

The obtained nanopaper was immersed in 0.2 g L^{-1} $AgNO_3$ aqueous solution to deposit a seed layer of Ag, and then immersed in a deionized aqueous solution and washed repeatedly. Finally, immersed a simple mixed solution of ammonia silver and glucose for 10 seconds to obtain conductive, transparent, and superhydrophobic cellulose film (CTSC-P).

2.6 Measurements and characterizations

The X-ray power diffraction (SAXSess mc2), scanning in the angular range of 20° to 80° (2θ), was used to detected the structures and pattern of silver on films. X-ray photoelectron spectroscopy (Thermo Fisher K-Alpha) was used to characterize the valence state of silver. Scanning electron microscope (SEM, Hitachi S4800) equipped with an energy-dispersive spectroscope (EDS, Oxford) was used to study the surface morphology of samples; atomic force microscope (AFM, BRUKER Dimension Icon) was used to measure the surface roughness. The contact angles and sliding angles were detected with a contact angle measurement instrument (SL200, China). A UV-vis spectrometer (4630F, Shanghai Yidian) equipped with an integrating sphere accessory was used to test the optical performances. The electric resistivity was measured using four-probe meter (RTS-4, Guangzhou Four-Point Probe Technology Co., Ltd). The cyclic voltammetry test was performed using princeton electrochemical workstation (PARSTAT-400, Princeton, America). The counter electrode was a platinum electrode with a size of 1×1 cm^2, the reference electrode was Ag/AgCl and the electrolyte solution was Na_2SO_4 (0.5 mol L^{-1}).

3. Results and discussion

3.1 Chemical structure and morphology

Wood has a multi-level structure, in which cellulose is the main component of the cell wall and plays the role of skeleton. It consists of micro-fibrils and micro-fibrils bundles. Different forms of nanocellulose can be prepared by chemical and physical methods. Sulfuric acid hydrolysis can deconstruct most of the amorphous area of the fiber, retain the crystalline area with strong resistance to degradation, and obtain short rod-shaped microcrystalline cellulose; cellulose fibrils with high aspect ratio and amorphous regions can be prepared through mechanical treatments such as high-pressure homogenization and ultrasonic dispersion. These nanocelluloses with different chemical structures and microscopic morphologies have potential applications in different fields.

In order to improve the transparency and mechanical strength of the substrate (cellulose films), in this study, TEMPO oxidation pretreatment combined with mechanical treatment were used to selectively oxidize the hydroxyl group at the C-6 position of the cellulose to a carboxyl group, during which the cellulose fibrils were decomposed into individual fibrils. As shown in Fig. 2b, the diameter of TEMPO oxidized cellulose (TOCNF) is about 7 nm. The high-density carboxyl groups introduced on the fibrils surface carry anionic charges in the water, and the electrostatic repulsion between TOCNF in the water can effectively act on the cellulose nanofibrils and promote a effective dissociation. The successful oxidation of the TOCNF was also further confirmed by the FTIR spectra (Fig. 2a). Compared with the cellulose, the FTIR spectrum of TOCNF showed a characteristic absorption peak of C=O in –COOH at 1732 cm^{-1}, indicating that a large number of carboxyl groups were introduced into the oxidized cellulose macromolecule.

The microscopic morphology of the cellulose films were characterized by SEM. The surface of TOC-P is smooth and compact relatively, and no obvious holes are observed (left two in Fig. 3a). The CNS is embedded in the surface of TOC-P to

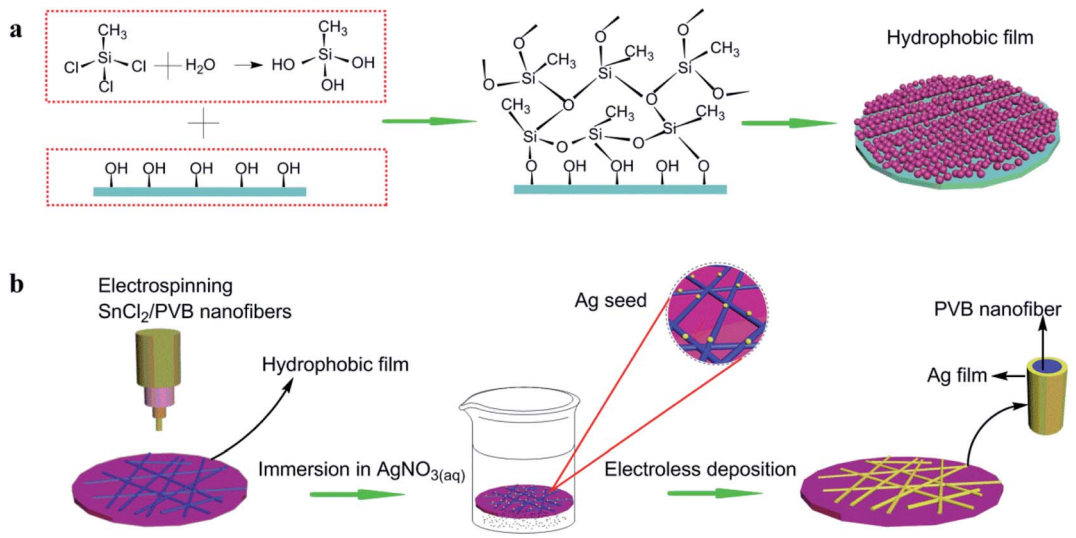

Fig. 1 Illustration of (a) reaction between methyltrichlorosilane and TOC-CNS-P. (b) Transparent, conductive cellulose film prepared by electrostatic spinning and electroless plating. First, PVB/$SnCl_2$ was electrospinned to form a nanowire network on TOC-CNS-P with a hydrophobic membrane, and then immersed in $AgNO_3$ solution to form activation points, during which Ag^+ was reduced to Ag simple substance. Finally, the activated sample was transferred to an electroless plating solution to form Ag nanowire network.

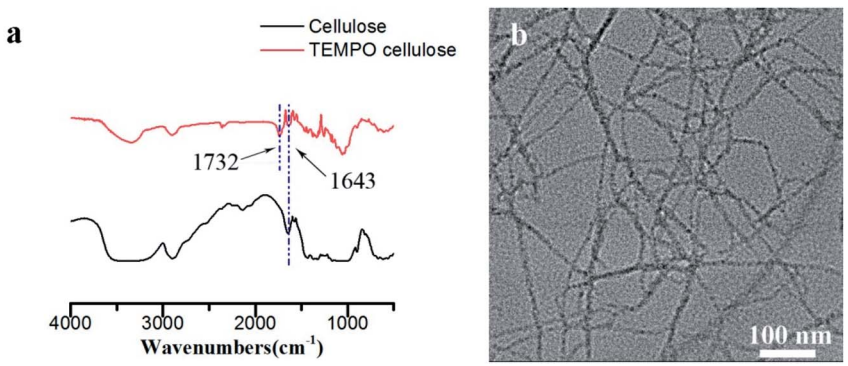

Fig. 2 (a) FTIR spectra of cellulose and TEMPO cellulose (b) TEM of TEMPO cellulose.

form a micron-level bump (right two in Fig. 3a), which provides a basis for the construction of a super-hydrophobic structure. The microscopic morphology of TOC-CNS-P changed significantly after superhydrophobic modification. Fig. 3b (left three) is the SEM image of the H-TOC-CNS-P sample obtained by MTCS treatment. It can be observed that the superhydrophobic modification has constructed a rough three-dimensional network of silane fibers on the surface of the TOC-CNS-P. The silane fiber has a "pearl necklace"-like structure, which is formed by connecting small silane balls. The porous silane network formed will significantly change the wettability of the film. In addition, the energy spectrum of Fig. 3b (rightmost) shows the distribution of Si on the surface of H-TOC-CNS-P, indicating that silane has a relatively uniform distribution on the surface of the film.

Fig. 1a shows a schematic diagram of the constructing polysilane fibers on the surface of TOC-CNS-P. The reaction process of MTCS and TOC-CNS-P is: trace water in the toluene solution hydrolyze with MTCS to form silanol, which further reacts with the hydroxyl groups on the surface of TOC-CNS-P to form new silanol. In addition, since silanol contains both hydrophilic group (–OH) and hydrophobic group ($-CH_3$), so it has self-assembly characteristics, which will cause the silane to continue to react with more Si–OH, thereby making the silane beads continue to grow with silane fibers, and finally "pearl necklace"-like silane fibers form a porous three-dimensional network structure on the surface of TOC-CNS-P.

Fig. 3c shows the scanning electron microscope (SEM) image of the chemically deposited Ag nanowire network and the corresponding energy dispersive spectroscopy (EDS) element map (right two). The green color in the EDS map represents the characteristic radiation of Ag element. Obviously, the film substrate passivated by the superhydrophobic treatment has little Ag deposition, due to the fact that the superhydrophobic passivated surface is difficult to contact the electroless plating solution to produce metallic silver. The Ag seed catalyst successfully promoted the grow of Ag coating along the nanowire network. The diameter of the nanowires used in our research is usually 600 nm. The diameter of the silver particles on the nanowire surface is about 20 nm.

To further confirm the existence of the silver network, the nanowire prepared by electrospuning PVB/$SnCl_2$ mixture were measured by X-ray photoelectron spectroscopy (XPS) after being oxidized by $AgNO_3$ (Fig. 4a). As is seen, after redox deposition, the presence of Ag^0 characteristic peak at 368.2 eV as directed by the Ag $3d_{5/2}$ peak in standard atlas suggested that Ag^+ ion had been reduced to Ag^0, and Ag seeds should generate and root in the surface of nanowire networks, which were beneficial to catalyze and promote the subsequent electroless silver plating reaction. The results of XPS are in good agreement with previous reports.[40] In addition, as shown in Fig. 4b, the X-ray diffraction (XRD) pattern further verified that the Ag precursor has been reduced onto the PVB/$SnCl_2$ nanowires. After $AgNO_3$ treatment, the XRD pattern of PVB/$SnCl_2$ nanowire network showed four obvious characteristic peaks, respectively are $2\theta =$ 38.39°, 44.26°, 64.64° and 77.58°, which correspond to (111), (200), (221) and (311) planes, proving the generation of Ag elementary substance with a face-centered cubic structure.

3.2 Optical properties

The optical performance of cellulose films are crucial to the wide application in optoelectronic devices, and its optical

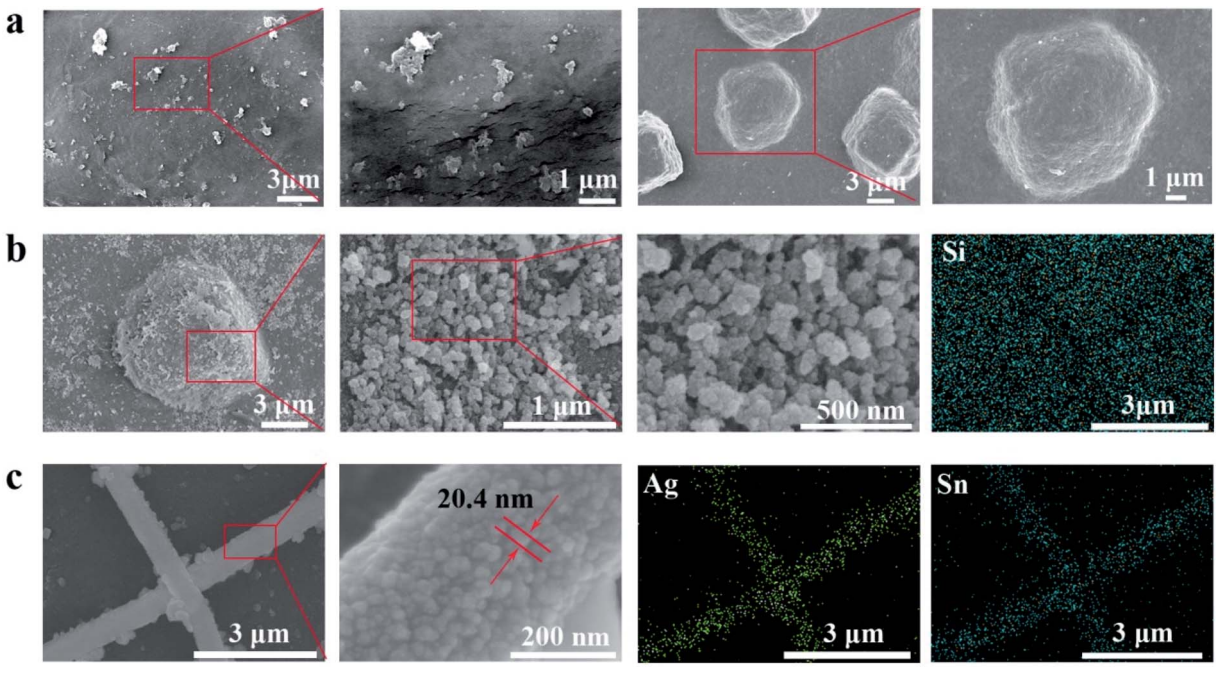

Fig. 3 The surface morphology of (a) TOC-P (left two) and TOC-CNS-P (right two). (b) H-TOC-CNS-P under SEM with different magnifications (left three) and elemental mapping of Si by EDS (rightmost). (c) CTSC-P under SEM with different magnifications (left three) and elemental mapping of Ag by EDS (rightmost).

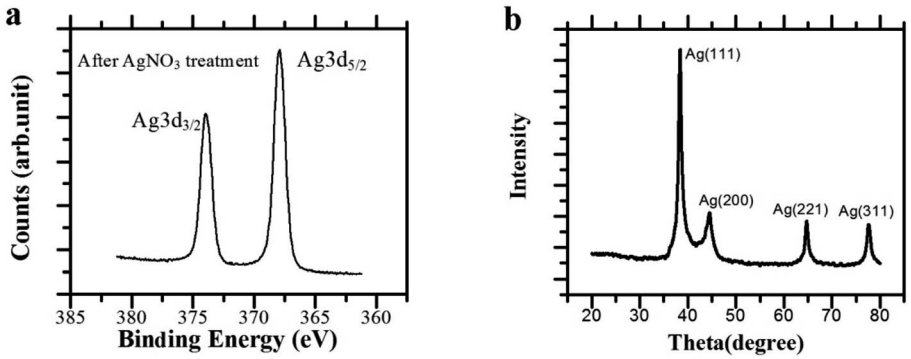

Fig. 4 (a) XPS spectra and (b) X-ray diffraction (XRD) pattern of nanowires network after $AgNO_3$ treatment.

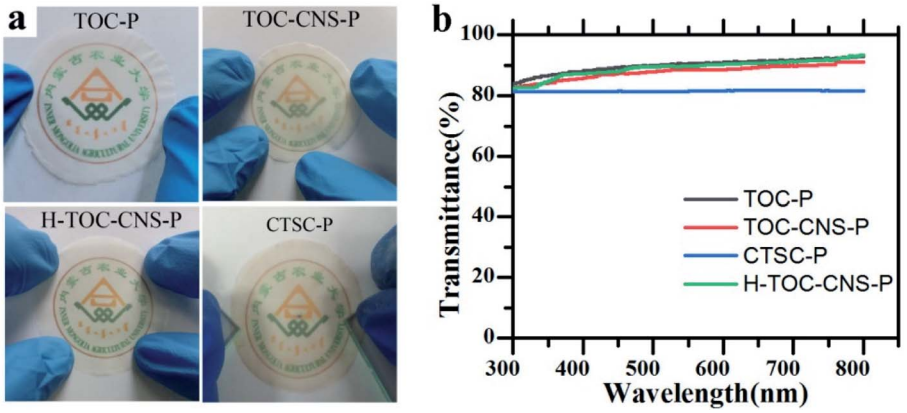

Fig. 5 Optoelectronic properties of TOC-P, TOC-CNS-P, H-TOC-CNS-P and CTSC-P. (a) Photos placed close to the school badge below. (b) The relationship between wavelength and transmittance.

properties are shown in Fig. 5. When the film is placed close to the image, the school's logo (Inner Mongolia Agricultural University) is clear, thus demonstrating high optical transparency. In addition, the relationship between wavelength and transmittance is shown in Fig. 5b. It can be seen that TOC-P shows the highest transmittance at 550 nm, which is 90.3%. A

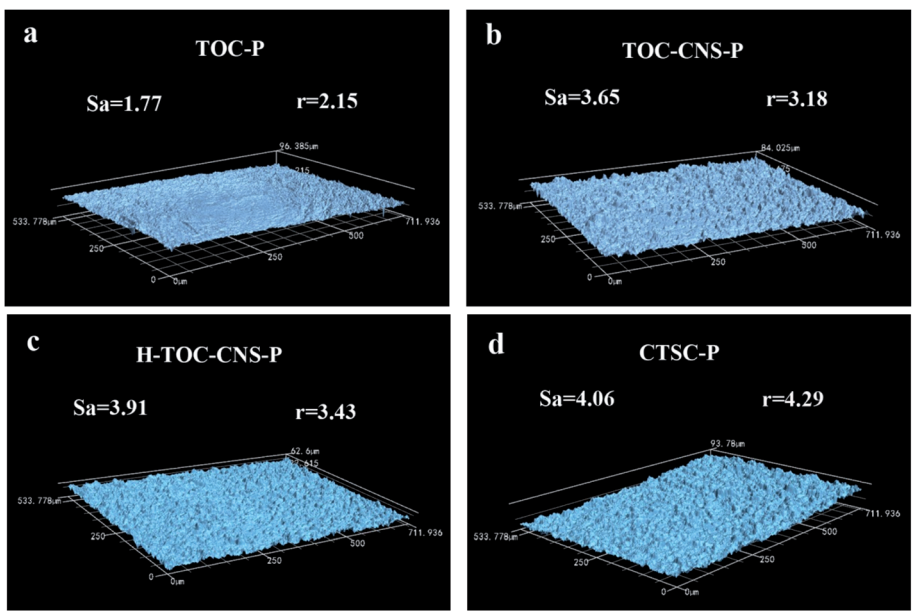

Fig. 6 Surface roughness of TOC-P, TOC-CNS-P, H-TOC-CNS-P and CTSC-P under laser scanning confocal microscope.

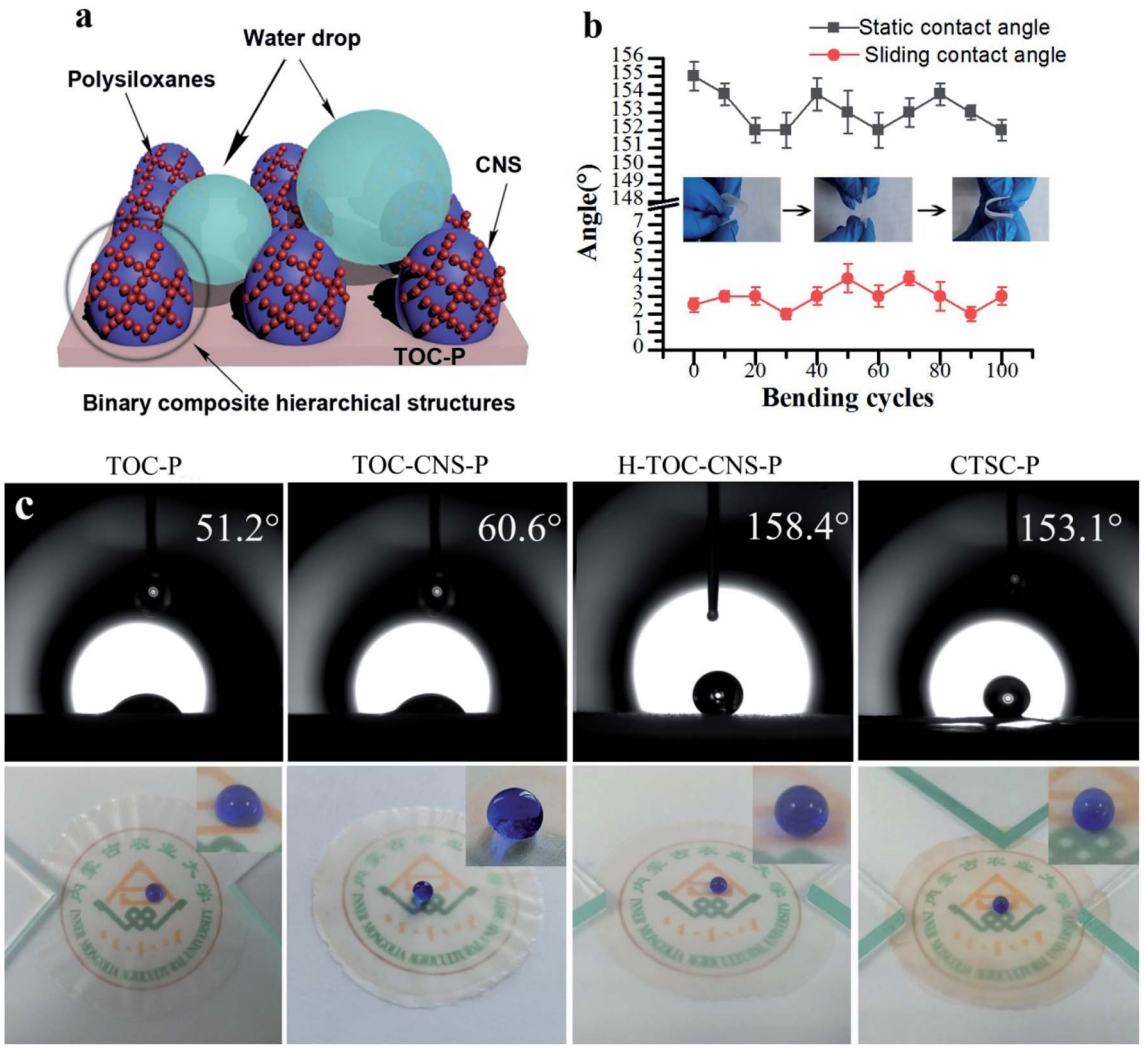

Fig. 7 (a) Illustration of water droplets on the superhydrophobic film. (b) The relationship between the bending cycles and water contact angles (CA)/sliding angles (SA). Inset in the chart showing the schematic of bending test. After 100 bending cycles, the surface still retain superhydrophobic properties. (c) Photos of TOC-P, TOC-CNS-P, H-TOC-CNS-P and CTSC-P with the water droplet on the surface.

possible explanation for this may be that each individual TEMPO cellulose fiber results in smaller forward scattering rather than significant back scattering because of its nanometer-scale diameter and micron-scale length. Therefore, the obtained dense multi-layer TOC-P allows most of the light to spread and retains proper light scattering. TOC-CNS-P has a high light transmittance (88.5% at a wavelength of 550 nm), which is close to TOC-P. This is because CNS guides the film surface to form a micron-level convex structure, thereby increasing the light diffuse reflection. The CTSC-P obtained after modification still maintains a high transmittance of 81.4% at 550 nm.

3.3 Surface wettability

As is known, superhydrophobic structure must be a rough surface covered by low surface energy substances. Therefore, the surface roughness is very important to the superhydrophobic structure. In Fig. 6, the roughness of TOC-P is the lowest at about 1.77 μm, while the roughness of TOC-CNS-P increased to 3.65 μm, which is attributed to the inlay of CNS on the surface of TOC. The surface roughness of H-TOC-CNS-P is further increased after the MTCS reaction, due to the production of many "pearl necklace"-like silane fibers on the surface of CNS. In addition, the surface of CTSC-P is covered by many silver nanoparticles, it is also conducive to the improvement of surface roughness. As to hydrophobicity, the roughness factor, r, which is defined as the ratio of the actual surface area to the projected surface area of CTSC-P, is 4.29. According to Pierre-Gilles de Gennes,[41] there is a threshold roughness for air retention ($r^* = 1.05$). When this threshold is exceeded, air pockets will be stuck in the rough surface area. Therefore, the surface roughness also contributes to hydrophobicity, besides light transmittance.

When the condensed water droplets fall on the superhydrophobic surface, they will stay on the curved surface, because the surface of the superhydrophobic coating has micro-

nano convex structures, which form many capillaries, as shown in Fig. 7a. CNS built micron-level raised structure on the surface of the film, which increases the roughness of the film.

Poor mechanical durability is a huge obstacle to the mass production of superhydrophobic films. As far as superhydrophobic film is concerned, the main consideration should be deformation and bending capability when received external force, rather than abrasion resistance. Fig. 7b shows the wettability in the bending area during multiple bending cycles. After 100 cycles of bending, the surface of film still has excellent water resistance (static contact angle >150°, sliding angle <5°), indicating good mechanical stability.

The wettability of TOC-P, TOC-CNS-P, H-TOC-CNS-P and CTSC-P was characterized by the static contactangles (CA) of the films (Fig. 7c). As is seen, H-TOC-CNS-P exhibited the highest water contact angles of 158.4°, proving the successful construction of superhydrophobic structure. The wettability of CTSC-P (about 153°) is lower than H-TOC-CNS-P. The reason is that hydrophilic silver element is deposited on the surface.

3.4 Electrical conductivity

Fig. 8a shows the $R_s - T$ relationship of the chemical deposition network. As far as we know, this $R_s - T$ performance (40.3 Ω

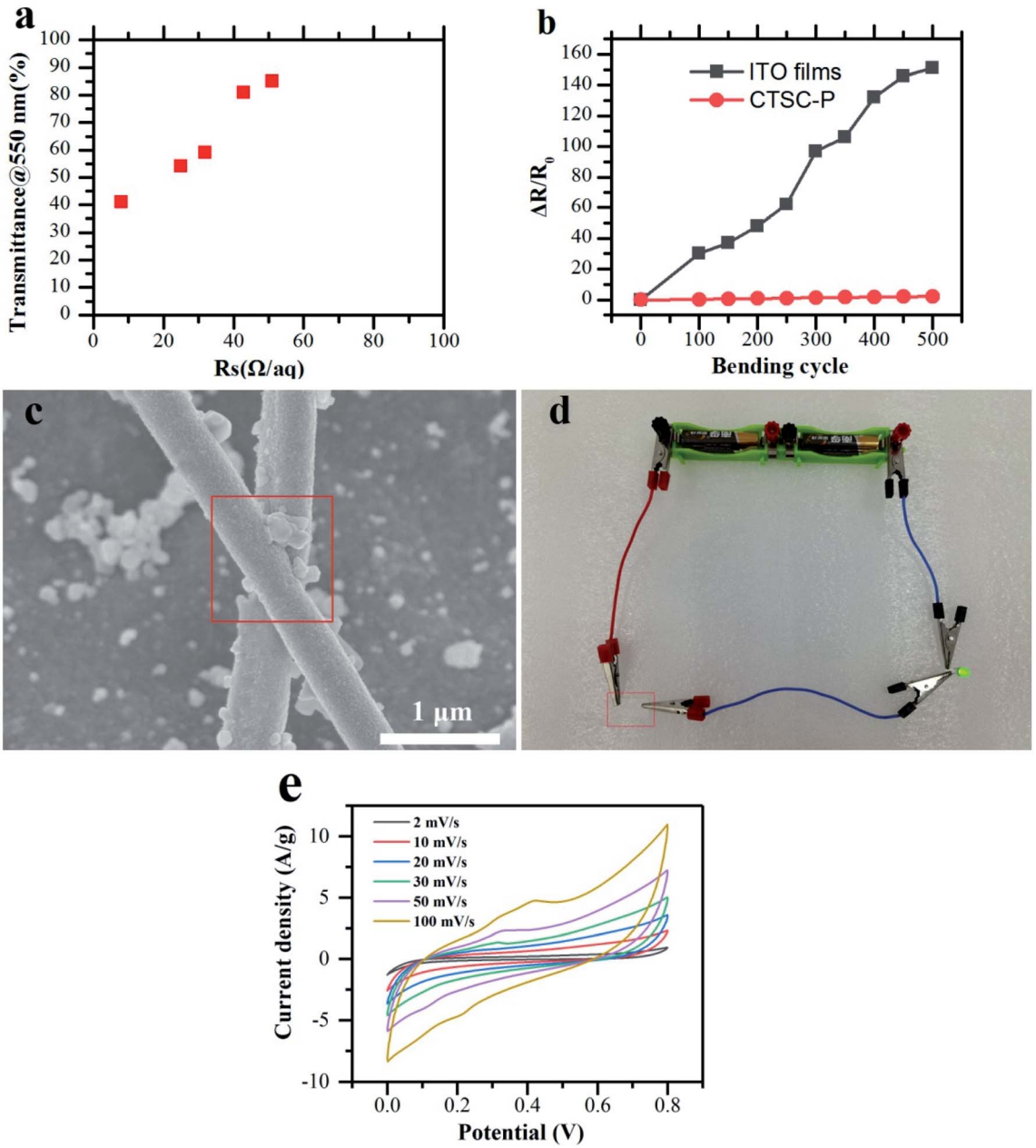

Fig. 8 Electrical conductivity of transparent, flexible, superhydrophobic cellulose films. (a) $R_s - T$ performance of CTSC-P. (b) Percentage sheet resistance change after 500 bending cycles. (c) SEM of Ag wire. The electroless despotion covers the whole junction, explaining the high performance of electricity. (d) Photo of CTSC-P with a power supply (2.3 V) lighting a green LED device. (e) CV curves at different scan rates of CTSC-P.

sq^{-1}) achieves performance comparable to ITO and enables the diode to emit light (Fig. 8d). This low resistivity is due to the reduced number of junctions between metal nanowires and lower junction resistance (Fig. 8c). Since electrospinning can prepare nanowires network with a length of centimeters, which is longer than a single solution-processed nanowire, it can easily achieve permeation threshold and continuous charge transport path.

In order to quantitatively show flexibility and durability of CTSC-P, the bending cycle test was carried out for up to 500 cycles, among which the bending radius is 4 mm (Fig. 8b). Under bending cycles, CTSC-P has better bending resistance compared to ITO films. The percentage change in the percentage resistance of the ITO film increased by about 150 times after 500 cycles, while the percentage of CTSC-P only increased by about 0.5 times. This significant difference in bending durability is that nano-sized metals have better ductility than metal oxides. Compared with conductive paper obtained by depositing metal nanowires, the junctions between metal nanowires have been fused during the electroless deposition process as is showed in Fig. 8c, and the whole process is completed at room temperature, therefore, has a wider range of applicability and application in flexible electronic products. In order to evaluate the electrochemical stability of CTSC-P electrode materials, the cyclic voltammetry (CV) test was performed, and the results are shown in Fig. 8e. Under different voltage scan rates, the CV curve basically maintains a rectangular-like shape, indicating that the electrode material has a faster current response under different voltages. As the scanning rate increases, the area of the CV curve becomes larger and larger, indicating that the electrode has excellent rate performance. This is because nano-Ag network provides a fast electron movement channel, which is conducive to the transmission of electrons on the surface and inside of the electrode. The rapid charge transfer provides the driving force for the material transfer between the electrode surface and the electrolyte.

4. Conclusions

In conclusion, we have developed a new multifunctional cellulose films that simultaneously realized high transmittance (81.4%), conductivity (R_s = 40.3 Ω sq^{-1}), and superhydrophobicity ($C_a = 153.2°$, $S_a = 4.1°$) for the first time.

Therefore, the cellulose film invented here is potentially feasible in a wide range of applications in flexible devices and even in functional devices such as wearable electronic devices, electronic display screens or other flexible electrode materials.

Author contributions

The manuscript was written through contributions of all authors. All authors have given approval to the final version of the manuscript.

Conflicts of interest

The authors declare no competing financial interest.

Acknowledgements

This work was support from the Science and Technology Plan Projects of Inner Mongolia Autonomous Region of China (No. 2021GG0074) and Grassland Talent Project in Inner Mongolia Autonomous Region.

References

1 M. Aryal, J. Geddes, O. Seitz, J. Wassei, I. McMackin and B. Kobrin, Sub-Micron Transparent Metal Mesh Conductor for Touch Screen Displays, *SID Int. Symp. Dig. Tech. Pap.*, 2014, **45**, 194–196.

2 R. D. Cairns, D. C. Paine and G. P. Crawford, The Mechanical Reliability of Sputter-Coated Indium Tin Oxide Polyester Substrates for Flexible Display and Touchscreen Applications, *MRS Proceedings*, 2001, **666**, F3.24.

3 H. Jeong, S. Park, J. Lee, P. Won, S. H. Ko and D. Lee, Fabrication of Transparent Conductive Film with Flexible Silver Nanowires Using Roll-to-Roll Slot-Die Coating and Calendering and Its Application to Resistive Touch Panel, *Adv. Electron. Mater.*, 2017, **4**, 1800243.

4 D. S. Hecht, K. A. Sierros, R. S. Lee, C. Ladous, C. Niu, D. A. Banerjee and D. R. Cairns, Transparent conductive carbon-nanotube films directly coated onto flexible and rigid polycarbonate, *J. Soc. Inf. Disp.*, 2011, **19**, 157–162.

5 Z. Liu, L. K. Ono and Y. Qi, Additives in metal halide perovskite films and their applications in solar cells, *J. Energy Chem.*, 2020, **46**, 216–228.

6 W. Han, G. Ren, Z. Li, M. Dong, C. Liu and W. Guo, Improving the performance of perovskite solar cells by surface passivation, *J. Energy Chem.*, 2020, **46**, 214–219.

7 Z. Muhammad, K. S. Ali, S. Fatima, A. Muddassir, M. Tareq, R. S. Abdur, K. W. Young, S. Mahmood and K. Do-Heyoung, Effect of Randomly Grown Morphology of ZnO Nanorods in Inverted Organic Solar Cells, *J. Nanosci. Nanotechnol.*, 2020, **20**, 4414–4418.

8 J. W. Han, B. Jung, D. W. Kim, K. T. Lim, S. Y. Jeong and Y. H. Kim, Transparent conductive hybrid thin-films based on copper-mesh/conductive polymer for ITO-Free organic light-emitting diodes, *Org. Electron.*, 2019, **73**, 13–17.

9 P. Pascal, S. Dominik, S. Simon, B. Carsten, S. Gintautas, H. Michael, V. Andrei and K. Holger, Optimization of Transparent Organic Light-Emitting Diodes by Simulation-Based Design of Organic Capping Layers, *J. Nanosci. Nanotechnol.*, 2019, **7**, 3959–3963.

10 J. Lee and Y. H. Kim, High performance ITO-free white organic light-emitting diodes using highly conductive PEDOT:PSS transparent electrodes, *Synth. Met.*, 2018, **242**, 99–102.

11 K. Ryu, X. Liu, E. Polikarpov, D. Zhang, J. Ly, M. E. Tompson and C. Zhou, Transparent, Conductive, and Flexible Carbon Nanotube Films and Their Application in Organic Light-Emitting Diodes, *Nano Lett.*, 2006, **9**, 1880.

12 H. W. Tien, Y. L. Huang, S. Y. Yang and S. T. Hsiao, Graphene nanosheets deposited on polyurethane films by

self-assembly for preparing transparent, conductive films, *J. Mater. Chem.*, 2011, **38**, 14876–14883.

13 Y. H. Wang, X. Yang, D. X. Du and X. F. Zhang, A comprehensive study of high-performance of flexible transparent conductive silver nanowire films, *J. Mater. Sci.: Mater. Electron.*, 2019, **14**, 13238–13246.

14 N. Wang, D. Xiong, S. Pan, Y. Deng, Y. Shi and K. Wang, Superhydrophobic paper with superior stability against deformations and humidity, *Appl. Surf. Sci.*, 2016, **389**, 354–360.

15 R. Xiong, Y. Han, Y. Wang, W. Zhang, X. Zhang and C. Lu, Flexible, highly transparent and iridescent all-cellulose hybrid nanopaper with enhanced mechanical strength and writable surface, *Carbohydr. Polym.*, 2014, **113**, 264–271.

16 K. B. R. Teodoro, F. L. Migliorini, M. H. M. Facure and D. S. Correa, Corrigendum to "Conductive electrospun nanofibers containing cellulose nanowhiskers and reduced graphene oxide for the electrochemical detection of mercury (II)", *Carbohydr. Polym.*, 2019, **207**, 747–754.

17 E. Shim, J. Su, J. Noro, M. A. Teixeira, A. Cavaco-Paulo, C. Silva and H. R. Kim, Conductive bacterial cellulose by in situ laccase polymerization of aniline, *PLoS One*, 2019, **4**, e0214546.

18 A. R. Rebelo, C. Liu, K. H. Schafer, M. Saumer and Y. Liu, Poly(4-vinylaniline)/polyaniline bilayer-functionalized bacterial cellulose for flexible electrochemical biosensors, *Langmuir*, 2019, **35**, 10345–10366.

19 A. B. A. Hammad, M. E. A. El-Aziz, M. S. Hasanin and S. Kamel, A novel electromagnetic biodegradable nanocomposite based on cellulose, polyaniline, and cobalt ferrite nanoparticles, *Carbohydr. Polym.*, 2019, **216**, 54–62.

20 J. He, N. Li, K. Bian and G. Piao, Optically active polyaniline film based on cellulose nanocrystals, *Carbohydr. Polym.*, 2019, **208**, 398–403.

21 M. Abdi, P. M. Tahir, R. Liyana and R. Javahershenas, A Surfactant Directed Microcrystalline Cellulose/Polyaniline Composite with Enhanced Electrochemical Properties, *Molecules*, 2018, **10**, 2470.

22 T. Kim, J. Kim, S. Hyun and S. M. Han, Fabrication of ultralight 3d porous composite for ag nanowire/cellulose nanofiber with tunable mechanical and electrical properties via directional freeze casting, *Extreme Mech. Lett.*, 2019, 100512.

23 D. Kim, Y. Ko, G. Kwon, U. J. Kim and J. You, Micropatterning Silver Nanowire Networks on Cellulose Nanopaper for Transparent Paper Electronics, *ACS Appl. Mater. Interfaces*, 2018, **10**, 38517–38525.

24 E. Ken, P. Huguette, N. Steven, D. Wim, L. Laurence, H. An and B. M. K. Van, Screen-printing of flexible semi-transparent electrodes and devices based on silver nanowire networks, *Nanotechnol.*, 2018, **42**, 5201.

25 H. Zhang, X. Sun, M. A. Hubbe and L. Pal, Highly conductive carbon nanotubes and flexible cellulose nanofibers composite membranes with semi-interpenetrating networks structure, *Carbohydr. Polym.*, 2019, **222**, 115013.

26 M. Jiang, R. Seney, P. C. Bayliss and C. L. Kitchens, Carbon Nanotube and Cellulose Nanocrystal Hybrid Films, *Molecules*, 2019, **14**, 2662.

27 H. Hosseini, M. Kokabi and S. M. Mousavi, Conductive bacterial cellulose/multiwall carbon nanotubes nanocomposite aerogel as a potentially flexible lightweight strain sensor, *Carbohydr. Polym.*, 2018, **201**, 228–235.

28 K. Zhang, L. Ketterle, T. Järvinen, S. Hong and H. Liimatainen, Conductive hybrid filaments of carbon nanotubes, chitin nanocrystals and cellulose nanofibers formed by interfacial nanoparticle complexation, *Mater. Des.*, 2020, **191**, 108594.

29 M. Zahid, E. L. Papadopoulou, A. Athanassiou and I. S. Bayer, Strain-responsive mercerized conductive cotton fabrics based on PEDOT:PSS/graphene, *Mater. Des.*, 2017, **135**, 213–222.

30 X. F. Zhang, L. Song, Z. Wang, Y. Wang, L. Wan and J. Yao, Highly transparent graphene oxide/cellulose composite film bearing ultraviolet shielding property, *Int. J. Biol. Macromol.*, 2020, **145**, 663–667.

31 J. Ampaiwong, P. Rattanawaleedirojn, K. Saengkiettiyut, N. Rodthongkum, P. Potiyaraj and N. Soatthiyanon, Reduced Graphene Oxide/Carboxymethyl Cellulose Nanocomposites: Novel Conductive Films, *J. Nanosci. Nanotechnol.*, 2019, **6**, 3544–3550.

32 H. Zou, X. Li, Y. Zhang, Z. Wang, B. Zhuo, T. Pu and Q. Yuan, Effects of different hot pressing processes and NFC/GO/CNT composite proportions on the performance of conductive membranes – Science Direct, *Mater. Des.*, 2020, **198**, 109334.

33 Y. Song, Y. Jiang, L. Shi, S. Cao, X. Feng, M. Miao and J. Fang, Solution-processed assembly of ultrathin transparent conductive cellulose nanopaper embedding AgNWs, *Nanoscale*, 2015, **32**, 13694–13701.

34 F. Hoeng, A. Denneulin, N. Reverdy-Bruas, G. Krosnicki and J. Bras, Rheology of cellulose nanofibrils/silver nanowires suspension for the production of transparent and conductive electrodes by screen printing, *Appl. Surf. Sci.*, 2017, **394**, 160–168.

35 Z. Zhang, H. Wang, S. Li, L. Li and D. Li, Transparent and flexible cellulose nanofibers/silver nanowires/acrylic resin composite electrode, *Composites, Part A*, 2015, **76**, 309–315.

36 R. Li, K. Zhang and G. Chen, Highly Transparent, Flexible and Conductive CNF/AgNW Paper for Paper Electronics, *Mater*, 2019, **2**, 322.

37 S. Chen, Y. Song and F. Xu, Highly Transparent and Hazy Cellulose Nanopaper Simultaneously with a Self-Cleaning Superhydrophobic Surface, *ACS Sustainable Chem. Eng.*, 2018, **6**, 5173–5181.

38 J. Xiong, S. Li, Y. Ye, J. Wang, K. Qian, P. Cui, D. Gao, M.-F. Lin, T. Chen and P. S. Lee, Transparent conductors: a deformable and highly robust ethyl cellulose transparent conductor with a scalable silver nanowires bundle micromesh, *Adv. Mater.*, 2018, **36**, 1802803.

39 L. R. Pederson, Comparison of stannous and stannic chloride as sensitizing agents in the electroless deposition of silver on glass using X-ray photoelectron spectroscopy, *Sol. Energy Mater.*, 1982, **2**, 221–232.

40 C. D. Wagner, L. H. Gale and R. H. Raymond, Two-dimensional chemical state plots: a standardized data set for use in identifying chemical states by X-ray photoelectron spectroscopy, *Anal. Chem.*, 1979, **4**, 466–482.

41 P. G. D. Gennes, F. Brochard-Wyart, Q. David, A. Reisinger and B. Widom, Capillarity and Wetting Phenomena: Drops, Bubbles, Pearls, Waves, *Am. Inst. Phys.*, 2004, 216–220.